PAPER

Check for updates

From trash to sensor: banana peel-derived silver nanocomposite as a mimic enzyme for cholesterol detection and antibacterial applications

Salman Ullah,[a] Muhammad Asad,[a] Farman Ullah,[b] Mohibullah Shah,[c] Khaled Fahmi Fawy,[d] Xiaoping Zhang,[e] Wei Sun,*[e] Umar Nishan [ID] *[a] and Amir Badshah*[a]

Cholesterol is the main building block of biological membranes and also a precursor of vitamin D, bile acids, and hormones. However, its abnormal concentration causes cardiovascular diseases, hypertension, hypothyroidism, and anemia. Therefore, it is crucial to keep a check on the amount of cholesterol in diet and blood serum. Herein we report a new, simple, and efficient colorimetric approach for the monitoring of cholesterol levels. In addition, the synthesized silver nanoparticles deposited over banana peel powder (Ag@bpp) were tested for their antibacterial potential against *Klebsiella pneumoniae* (*K. pneumoniae*), *Escherichia coli* (*E. coli*), *Staphylococcus aureus* (*S. aureus*), and *Pseudomonas aeruginosa* (*P. aeruginosa*). The nanozyme was prepared by simple reduction in a basic medium over the surface of banana peel powder (bbp) and characterized by various spectroscopic and morphological techniques. The Ag@bpp showed both oxidase and peroxidase enzyme-like activities simultaneously without the use of external hydrogen peroxide. The hydrogen peroxide produced as a result of oxidation of cholesterol could oxidize 3,3′,5,5′-tetramethylbenzidine (TMB) to produce a blue-green colored product, oxidized TMB (oxTMB). Besides this observable colorimetric change, it was also confirmed by a UV-visible spectrophotometer in terms of absorbance to find the exact concentration of cholesterol. The optimized conditions were found to be 1.8 mg of the mimic enzyme, pH 5, TMB 4 mM, and 4 minutes of incubation time. The fabricated sensor displayed a linear range for the analyte in the range of 2–20 mM with a 0.029 mM limit of detection. The nanozyme was also successfully applied for cholesterol detection in human serum samples with excellent reproducibility. The synthesized nanocomposite also showed excellent inhibitory effect against various bacterial strains. These findings prove that the synthesized nanocomposite is not only effective in colorimetric detection of cholesterol but also has strong antibacterial activities.

1. Introduction

Cholesterol is a vital lipid molecule in the human body. It is an essential component of animal cell membranes and helps to maintain membrane structural integrity and fluidity. It is also considered a precursor for the production of vitamin D, bile acids, and steroid hormones. Since cholesterol plays a vital role in animal physiology, all cells have the enzymatic resources needed to synthesize it from simpler chemical precursors.[1] The ideal level of cholesterol in a healthy human serum has been reported to be 200 mg dL^{-1}.[2] On the other hand, cholesterol in the blood serum is linked to various diseases such as plaque accumulation in the arteries, which narrows and hardens the arteries, resulting in less blood supply to the heart, brain, and other essential organs. This elevates the risks of coronary artery disease as well as cardiovascular mortality.[3,4] In addition, the high level of cholesterol can cause hypertension and cancer in the human body.[5] Abnormally low levels of cholesterol in blood serum can also cause a medical disorder known as hypocholesterolemia, which may cause stroke and liver cancer.[6] All this makes it necessary to monitor the level of cholesterol through reliable, sensitive, selective, point-of-care, portable, easy-to-use, and low-cost platforms.

The detection and quantification of cholesterol have previously been reported through various techniques such as fluorescence,[7] electrochemical,[8,9] molecular imprinting,[10] chromatographic,[11,12] field effect transistor,[13] and

[a] Department of Chemistry, Kohat University of Science and Technology, Kohat 26000, KP, Pakistan. E-mail: umarnishan85@gmail.com; amirqau@yahoo.com

[b] Department of Pharmacy, Kohat University of Science and Technology, Kohat 26000, KP, Pakistan

[c] Department of Biochemistry, Bahauddin Zakariya University, Multan 66000, Pakistan

[d] Department of Chemistry, Faculty of Science, Research Center for Advanced Materials Science (RCAMS), King Khalid University, P.O. Box 960, Abha, 61421, Saudi Arabia

[e] Hainan International Joint Research Center of Marine Advanced Photoelectric Functional Materials, College of Chemistry and Chemical Engineering, Hainan Normal University, Haikou 571158, P. R. China. E-mail: sunwei@hainnu.edu.cn

chemiluminescence methods.[14] Although the mentioned techniques offer several merits, they are costly to acquire and sustain, difficult to handle and operate, and may require complex sample pretreatment steps.[15,16] Therefore, it is necessary to develop a straightforward, rapid, inexpensive, sensitive, specific, and easy-to-use method for the detection and quantification of cholesterol.

The colorimetric method offers an alternative approach in comparison to the aforementioned techniques. It has numerous advantages, such as simple use and no need for expensive apparatus and skilled operators. It is rapid, and the progress of its reaction can be observed through the naked eye.[17–19] Traditionally, colorimetric sensor technology development relied on the use of natural enzymes such as horseradish peroxidase and alkaline phosphatase, *etc.* The use of these enzymes resulted in the increased vulnerability of the colorimetric sensors in that era because of the shortcomings of natural enzymes.[20] However, the known shortcomings of natural enzymes, namely pH and temperature sensitivity, low shelf life, difficult handling, and high cost, resulted in the decreased viability of colorimetric sensors.

However, the use of iron oxide nanoparticles as enzyme mimics opened a new avenue for future developments in colorimetric sensor technology.[21–23] The explosive growth in nanotechnology and nanomaterials development has provided a much-needed impetus for the development of portable, tunable, low-cost, easy-to-use, thermally stable colorimetric sensing platforms.[24–26] It has resulted in a renaissance of this technology that had become stagnant for a period of time. The nanomaterial-based sensor technology heavily relied on the use of noble metal elements such as Pt, Pd, Au, and Ag. Among them, Ag is the most cost-effective by far comparatively. Other metals and their oxides, although more cost-effective, are less efficient in terms of performance and reliability. The current work therefore opted to use Ag, as it hits the perfect balance in terms of cost and efficiency. Ag itself is not immune from problems, and its pristine form, owing to its high surface energy, is prone to agglomeration.[18,27] It results in loss of surface area and a drastic loss in its activity and efficacy. This needs to be overcome by the use of some form of passive materials. Various synthetic and biocompatible options can be explored for this purpose. Biocompatible passive materials are preferable over their synthetic counterparts, as they are friendly to the environment, cost-effective, and ubiquitous.

In this regard, banana peel can be used as a source of passive materials that fulfills the criteria of environmental friendliness, low or no cost, and abundant availability. Banana peel is of significant interest because it is a fruit globally available and is considered to be the fourth most abundant. Its peel under normal circumstances is thrown away and apparently carries no economic value. Its peel is a rich source of various bioactive compounds, which are helpful in the reduction of metal salts alongside the stabilization of nanoparticles. Therefore, it has been previously used for the removal of dyes, pesticides, heavy metals, and various industrial pollutants.[28–30] Various nanomaterials systems have been used for the colorimetric determination of cholesterol such as AuNPs@DACNFs,[31] Fe_3O_4-GBR,[32] MOFs,[33] and NSC/Co_{1-x}S.[34]

K. pneumoniae, *E. coli*, *S. aureus*, and *P. aeruginosa* are frequently implicated in a diverse range of diseases. The growing trend of microbial resistance makes it necessary to explore and report on new potential antimicrobial agents.[35,36] The current work is one such attempt, which tries to unveil the antimicrobial potential of the synthesized nanocomposite.

The novelty of the work lies in the synthesis of silver-deposited banana peel powder (Ag@bpp) as a colorimetric sensing platform for the sensing and estimation of cholesterol. All the characterization confirmed the desired synthesis of the nanocomposite with excellent dispersion of silver nanoparticles achieved over the matrix of bpp. The sensing system demonstrated excellent sensitivity and selectivity for cholesterol detection and quantification in the presence of chromogenic substrate (TMB) without the use of hydrogen peroxide. The fabricated sensor was successfully applied for the detection of cholesterol in real samples.

2. Experimental

2.1. Chemical and material

All the chemicals, including cholesterol, tetramethylbenzidine, sodium hydroxide, monobasic sodium phosphate, disodium hydrogen phosphate, glucose, hydrochloric acid, hydrogen peroxide, dopamine, uric acid, ascorbic acid, glycine, and tyrosine, were purchased from Sigma Aldrich, USA. All the chemicals were used without any further purification steps and used as received. Locally, lab-produced deionized water was used for the preparation of solutions during the experiments. Banana peels were obtained from a fruit shop located near Kohat University, Khyber Pakhtunkhwa, Pakistan.

2.2. Instrumentation

Fourier transform infrared spectroscopy (FTIR) was conducted using an Agilent Technologies FTIR spectrometer MA 5700 in the range of 4000 to 500 cm^{-1}. By the use of a ZEISS Gemini 500 Germany scanning electron microscope (SEM) coupled to EDS, the surface morphology and elemental composition were studied. A Bruker AXS D8 X-ray powder diffractometer was used to study the crystalline phase of the nanocomposite. To get further insight into the morphology and surface chemical state of the synthesized nanocomposite, a JEM-2100F microscope (JEOL, Japan) and X-ray photoelectron spectroscopy (XPS) Thermo, USA were used for HRTEM and XPS analysis, respectively. A UV-visible spectrophotometer (Shimadzu UV, 1800, Japan) was used throughout the work to record the absorption spectra.

2.3. Synthesis of the banana peel powder and nanocomposite

The banana peels were carefully washed using double distilled water to remove dust and any other impurities from their surface. They were shade-dried for two weeks in open air and ground to fine powder. The powder was sieved using several mesh sizes, and the fraction sizing 300–500 μm was collected and stored for further use. For the preparation of Ag@bpp, 0.025 M, 100 mL solution of AgNO₃ and 4 grams of bpp were taken and blended

for one hour to obtain a homogenous mixture. To this mixture, 40 mL of 0.025 M NaOH solution was added dropwise and kept under constant stirring for two hours until complete precipitation occurred. As a result of this, a precipitate containing Ag@bpp was obtained. The precipitate was filtered and washed several times through double-distilled water to achieve neutral pH. Finally, the prepared material was dried for six hours at 80 °C in an oven and used in onward experiments.

2.4. Colorimetric detection of cholesterol

For the colorimetric detection of cholesterol, various amounts of the synthesized nanozyme were tested in the presence of TMB, phosphate buffer saline, and the analyte and incubated for a specific period of time. After a while a colorimetric change was visible to the naked eye, and the image was captured through a smartphone. This change in color was confirmed through a UV-Vis spectrophotometer. In the first experiment, bpp was used alongside the other constituents of the sensor system, such as TMB, phosphate-buffered saline, and the analyte. The result was observed, and confirmation was carried out through spectrophotometry. In the second experiment the prepared nanocomposite (Ag@bpp) was tested instead of pristine bpp in the absence of cholesterol. The change was monitored through spectrophotometry and the naked eye. Finally, in the third experiment, cholesterol (analyte) was introduced into the mixture of the proposed mimic enzyme, buffer solution, and TMB and incubated for a certain period of time. Again, the progress of the reaction was monitored, images were captured through smartphone, and confirmation was obtained through spectrophotometry. The reactions were carried out using 2 mg of the mimic enzyme, 550 μL of PBS buffer at pH 4.5, 80 μL of 4.5 mM TMB, and 120 μL of 22 mM cholesterol and incubated
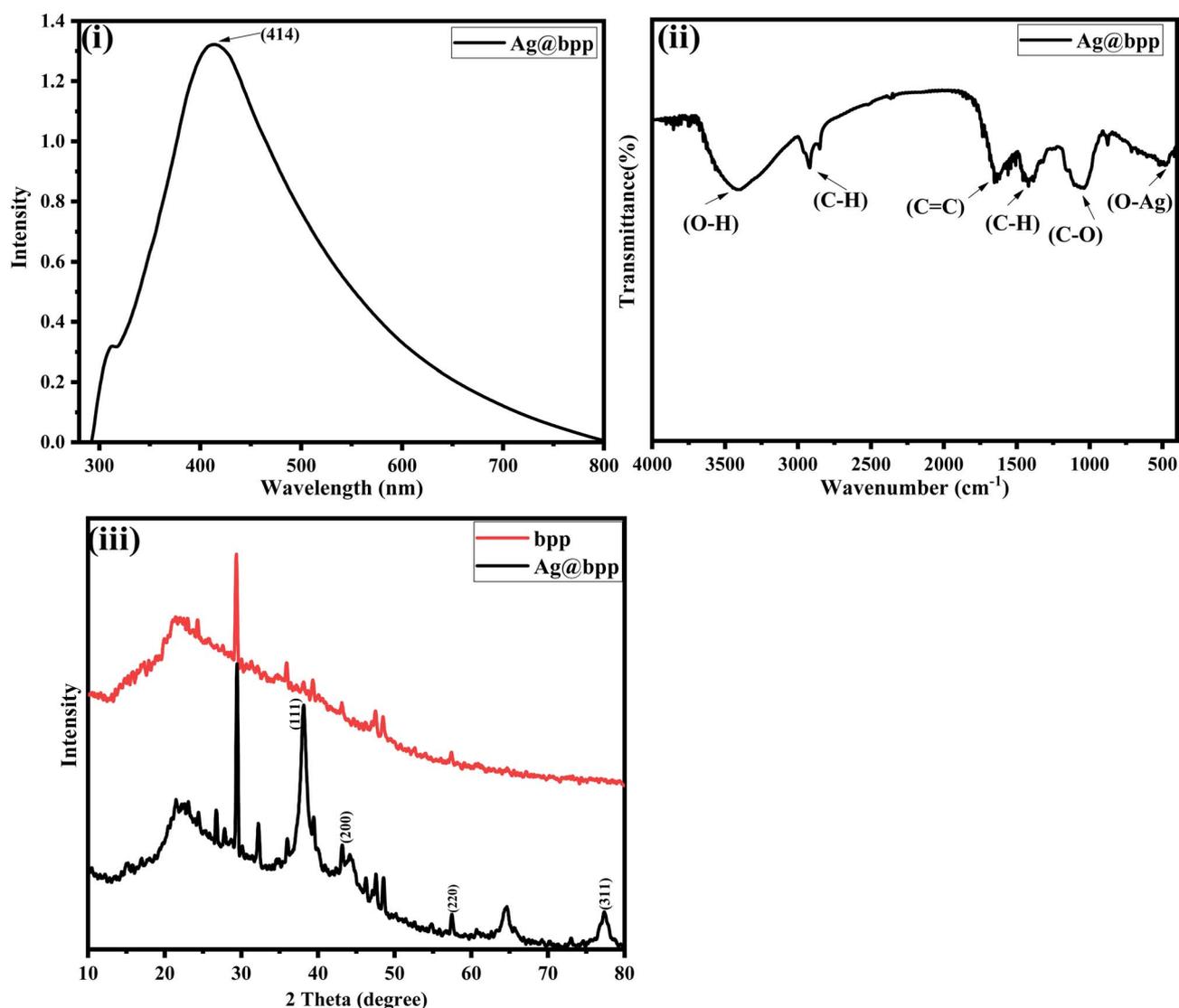

Fig. 1 (i) shows the UV–visible spectroscopy peak of Ag nanoparticles at $\lambda_{max} = 414$ nm in line with literature. (ii) show the FTIR spectrum of Ag@bpp demonstrating the characteristic peaks of bpp and an extra peak for Ag in the fingerprint region. (iii) show the XRD analysis of bpp and Ag@bpp corresponding to the presence of lattice planes assigned to silver.

for 5 minutes. The work was approved from the ethical committee of Kohat University through Approval No. KUST/Ethical Committee/1628.

2.5 Antimicrobial activities

Four bacterial strains, *Klebsiella pneumoniae* (*K. pneumoniae*), *Escherichia coli* (*E. coli*), *Staphylococcus aureus* (*S. aureus*), and *Pseudomonas aeruginosa* (*P. aeruginosa*), were selected for the current study. Firstly, the bacterial strains were grown in Mac-Conkey agar, mannitol salt agar, and Mueller–Hinton agar (MHA) for 24 hours to obtain fresh cultures. Next, isolated colonies of each culture were selected. A cotton bud was used to delicately transfer a small colony of each strain to a Petri dish containing the MHA. After spreading the inoculum equally, it was left to stick to the agar surface for 20 minutes. Then, five wells (6 mm diameter) were made for testing the activity, and two positive controls were also applied. After that, 100 μL of

2 mg mL^{-1} of the Ag@bpp was applied to well no. 1, and 100 μL of 1 mg Ag@bpp was applied to well no. 2. Well no. 3 and 4 were used for the application of banana peel powder (BPP). Two positive control disks, imipenem (10 μg) and gentamicin (10 μg), were used for comparison. DMSO 100 μL was used as a negative control throughout the experiments. Finally, the Petri dishes were incubated for 24 hours at 35 °C. After 24 hours the Petri dishes were observed, and the inhibition zone was compared to positive controls.

3. Results and discussion

3.1. Characterization

3.1.1. Spectroscopic analysis of the synthesized material.
The prepared Ag@bpp nanocomposite was characterized through various spectroscopic techniques to unveil its successful synthesis. Firstly, UV-visible spectroscopy results
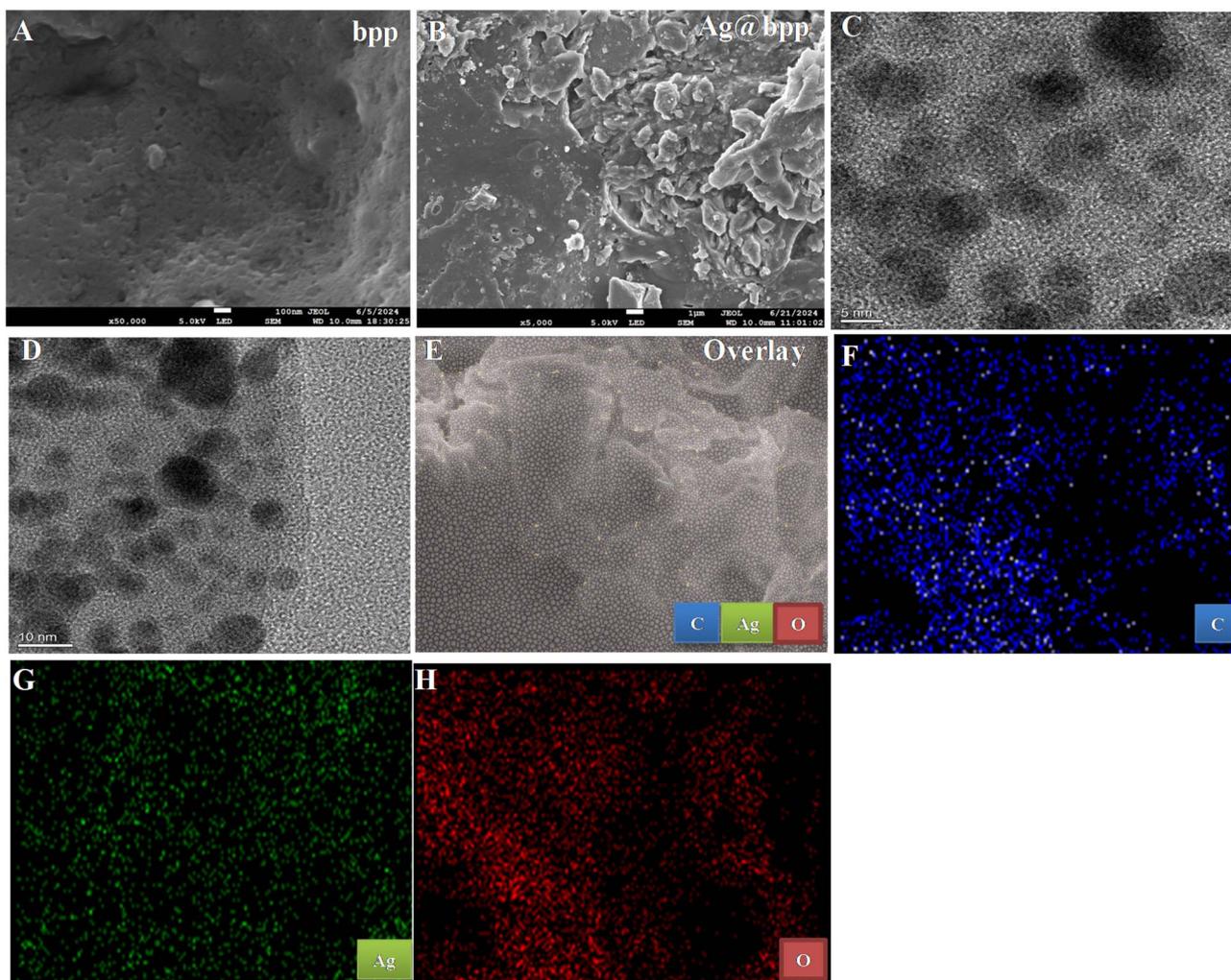

Fig. 2 Image (A) shows the surface characteristics of banana peel powder with a plain and porous surface morphology. (B) show the SEM image of the synthesized Ag@bpp with a rough surface showing the deposition of Ag on the surface of bpp. Images (C) and (D) show the HRTEM results with the uniform distribution of the Ag nanoparticles over the surface of the passive materials of bpp. (E) show the overlay of elemental mapping of prepared material containing all the main elements present in the synthesized Ag@bpp. Images (F)–(H) show the elemental distribution of the constituent elements such as carbon (C), silver (Ag), and oxygen (O) on the surface of bpp.

showed an intense peak at λ_{max} of 414 nm for the nano-composite, as shown in Fig. 1(i). The surface plasmon resonance of the synthesized nanocomposite falls in line with the already reported value for Ag nanoparticles.[37] The FTIR results revealed a pattern similar to that of already published FTIR for banana peel powder previously by our group.[38] However, there was a small extra peak for Ag@bpp in the fingerprint region, which could be ascribed to silver, indicating its deposition on the bpp. Briefly, as can be seen in Fig. 1(ii), the band around 3430 cm^{-1} can be attributed to the presence of the OH group present in the compounds of bpp. The peaks around 2922 and 2856 cm^{-1} can be assigned to –CH$_2$– and –CH$_3$ groups in the synthesized material. A small, sharp peak at 1740 cm^{-1} indicates the carboxyl group of aliphatic carboxylic acids or their esters in banana peels. The absorption band around 1645 cm^{-1}

indicates aromatic C=C stretching vibration of the bpp.[39] The bending vibration of the C–H was observed at 1422 cm^{-1} in accordance with reported literature.[29] The peak at 1060 cm^{-1} indicates the presence of ether linkage in the compounds present in the bpp.

The crystalline nature of both bpp and Ag@bpp nanocomposite was studied through X-ray diffraction analysis in the range of $2\theta = 10$–$80°$. The crystallinity in the structure of bpp can be attributed to the presence of cellulose, lignin, and amorphous hemicelluloses,[40] as shown in Fig. 1(iii). The extra peaks in the XRD pattern of the synthesized Ag@bpp observed at 38.10°, 44.20°, 64.40°, and 77.50° correspond to the planes (111), (200), (220), and (311), respectively. These peaks correspond to the JCPDS, No. 04-0783, as reported earlier in literature.[41] This confirms the successful deposition of Ag on the
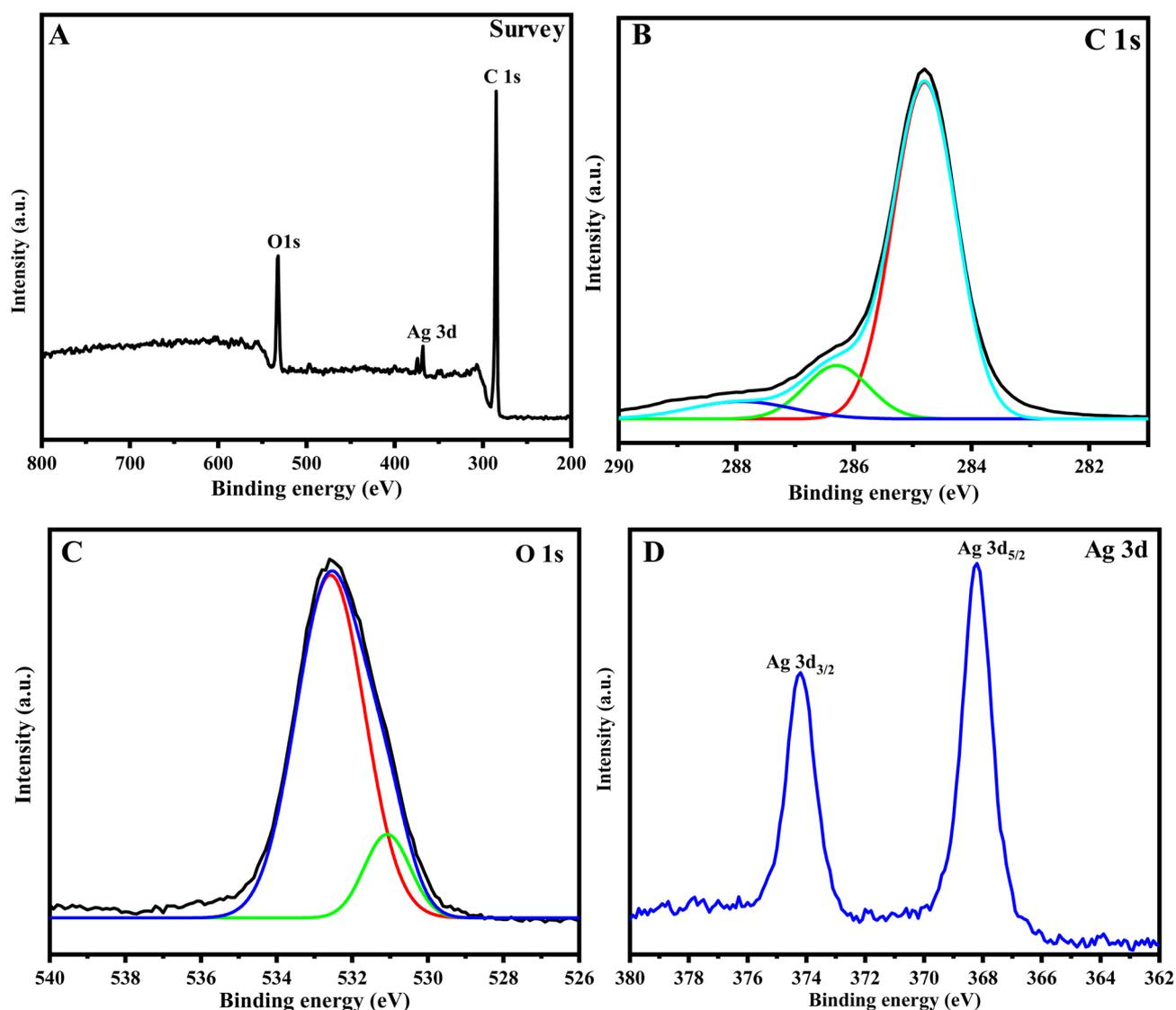

Fig. 3 (A) represents the survey spectrum indicating the presence of O 1s, Ag 3d, and C 1s. (B) The deconvoluted spectrum of C 1s shows peaks at 284.6 eV, 286.4 eV, and 287 eV that represent C=C/C–C, C–O, and C=O. (C) shows the deconvoluted spectrum of O 1s representing C–O at a binding energy of 531 eV and C=O at a binding energy of 532.8 eV. (D) represents the presence of Ag$^+$ and Ag^0 at their respective binding energies.

surface of bpp. Using the Scherrer equation, the crystallite size of the nanocomposite (Ag@bpp) was calculated to be 35.25 nm.

3.1.2. Surface morphology of the prepared materials. The morphological characteristics of the synthesized bpp and Ag@bpp were investigated using different techniques as shown in Fig. 2. SEM images of bpp and Ag@bpp are shown in Fig. 2A and B, respectively. There were crater-like pores on the surface of the natural banana peel powder, giving it an irregular shape. The porous surface of banana peel powder enables effective deposition of silver nanoparticles over the surface of bpp.[42] Fig. 2B illustrates the rough surface morphology, confirming the successful deposition of Ag nanoparticles onto the surface of bpp. For deeper understanding of the morphology of the synthesized material, high-resolution transmission electron microscopic analysis of the synthesized Ag@bpp

nanocomposite was performed. HRTEM analysis revealed that the synthesized silver nanoparticles deposited on bpp were spherical in shape. The passive material of bpp is providing an excellent surface to the Ag and immobilizes it to prevent its agglomeration, as shown by images (C) and (D) in the figure. Further morphological analysis was performed through elemental mapping to ascertain the distribution of the constituent elements in the synthesized Ag@bpp nanocomposite as shown through images (E)–(H) in the figure. Image (E) depicts the overlay of all the constituent elements of the synthesized nanocomposite. Whereas images (F), (G), and (H) show the distribution of carbon (C), silver (Ag), and oxygen (O), respectively. From the images it is clear that the distribution of the constituent elements of the Ag@bpp nanocomposite is uniform and homogenous. This also confirms that the passive material of bpp provides an excellent anchoring surface area for the immobilization of the Ag nanoparticles to keep its surface area intact. In the absence of passive materials, the nanoparticles, owing to their high surface area, would have come together and would have lost their activity to a greater extent. This confirms the important role of the otherwise waste banana peel powder in a very useful application.

3.1.3. XPS analysis of the synthesized nanocomposite. X-ray photoelectron spectroscopy was used to study the composition and surface chemical state of the elements present in the synthesized nanocomposite. Fig. 3A shows the survey spectrum of the Ag@bpp, indicating the presence of oxygen, silver, and carbon. In order to get further details, the spectrum was deconvoluted for the constituent elements. Fig. 3B illustrates the deconvoluted spectrum of C 1s with three peaks with binding energy values at 284.6 eV, 286.4 eV, and 287 eV that represent C=C/C–C, C–O, and C=O.[43,44] The spectrum of O 1s is shown in Fig. 3C, which revealed two distinct oxygen states, corresponding to C–O at a binding energy of 531 eV and C=O at a binding energy of 532.8 eV.[45,46] Fig. 3D shows the deconvoluted spectrum of the Ag 3d region, revealing the presence of two distinct oxidation states of silver. The binding energy values centered at 374 eV and 368 eV correspond to Ag $3d_{3/2}$ and Ag $3d_{5/2}$, respectively. These values represent the presence of Ag^+ and Ag^0 species in the synthesized nanocomposite.[47]
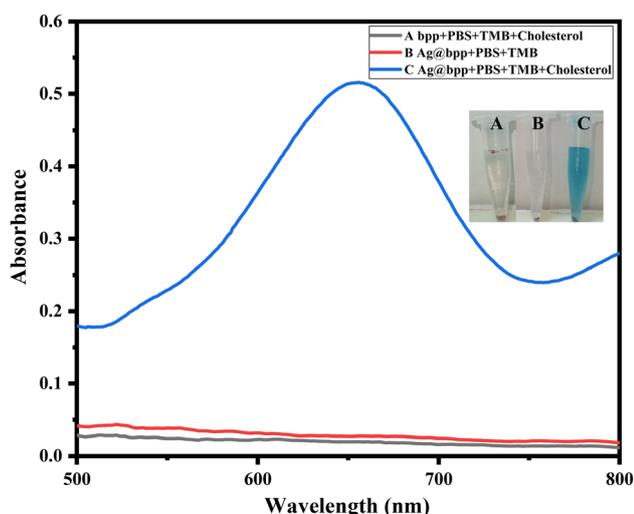

Fig. 4 Shows the colorimetric detection of cholesterol through the synthesized Ag@bpp nanozyme system. (A) shows that bpp alone in the presence of other constituents cannot detect the analyte under study. (B) indicate that the Ag@bpp, TMB solution, and PBS buffer show no reaction in the absence of cholesterol. (C) shows that the combination of Ag@bpp, TMB solution, PBS buffer, and cholesterol results in a visible colorimetric change.
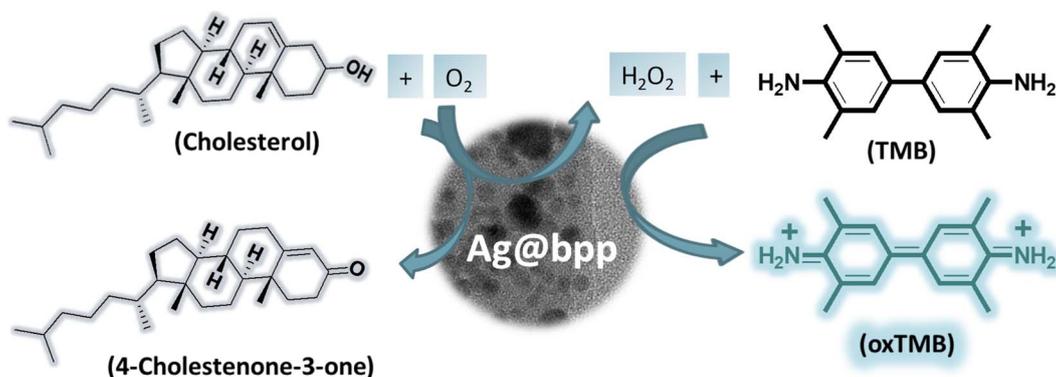
Scheme 1 Demonstrates the role of the synthesized Ag@bpp nanocomposite in the sensing of cholesterol without the use of external hydrogen peroxide.
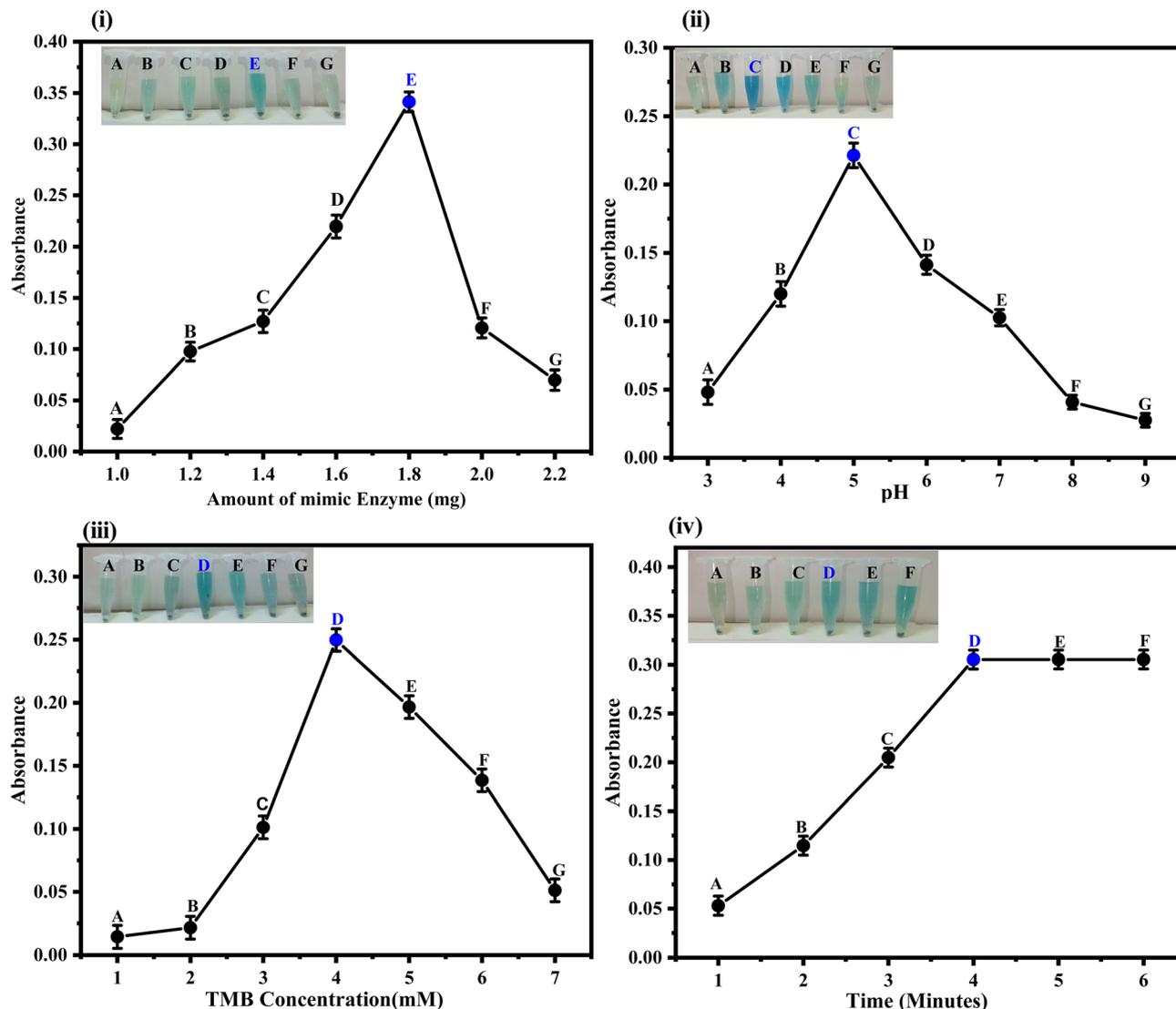
Fig. 5 Shows the optimization results of various parameters that influence the activity of the fabricated sensor. (i) demonstrate the optimization results of the amount of nanozyme in the range of 1–2.2 mg, with optimal response observed at 1.8 mg. (ii) Depicts the pH optimization results, and the best response was seen at pH 5. (iii) illustrate the results achieving the best response at 4 mM TMB. (iv) show time optimization with the best optical change was seen at 4 minutes. The reaction conditions were [1.8 mg of the Ag@bpp, PBS 400 μL (pH 5), TMB 80 μL (4 mM), time 4 minutes, and cholesterol 100 μL (20 mM)].

3.2. Colorimetric detection of cholesterol

As mentioned in the Experimental section, in the first experiment bpp was used along with TMB, and PBS buffer. The

Table 1 Comparative analysis of the peroxidase-like activity of the nanozyme Ag@bpp and HRP, which acts as a natural peroxidase

Catalyst used	Substrate used	V_{max} (10^{-8} M s^{-1})	K_m (mM)	Reference
HRP	TMB	10.19	0.424	48
HRP	H_2O_2	10.55	3.24	
Ag@bpp	TMB	8.34	3.95	This work
Ag@bpp	H_2O_2	9.43	4.68	

addition of cholesterol to this mixture resulted in no colorimetric change as noted through Eppendorf tube A and curve A. In the second experiment the synthesized mimic enzyme Ag@bpp was used alongside TMB and PBS buffer. After incubation for a period of 5 minutes, no change in color could be observed, as noted through Eppendorf tube B and curve B. In this experiment, the analyte was not incorporated into the system. In the third and final experiment, the proposed mimic enzyme (Ag@bpp), TMB solution, PBS buffer, and cholesterol were combined together and incubated for 5 minutes. An intense blue-green color characteristic of oxTMB was visible to the naked eye, and confirmation was performed through spectrophotmetry, as can be seen in Eppendorf tube C and curve C (Fig. 4).

3.3. Proposed mechanism for the detection of cholesterol

The as-synthesized nanocomposite (Ag@bpp) acted as a tandem nanozyme. The synthesized nanozyme showed oxidase (chOx) and peroxidase-like activities simultaneously under the same conditions, as shown in Scheme 1. First of all, the cholesterol was oxidized to 4-holestenone-3-one by the action of the nanozyme in the presence of oxygen. At the same time, H_2O_2 is generated as a byproduct during the course of this reaction. The nanozyme simultaneously decomposed the generated H_2O_2 in the following reaction to produce peroxide radical ($^{\cdot}OH$), indicating its peroxidase-like activity. The generated $^{\cdot}OH$ can oxidize the TMB to oxTMB. This oxidation resulted in enhanced conjugation and thus reduced the energy gap between the frontier orbitals. Due to which the absorption is shifted to the visible region, *viz.*, blue-green. This visible observation was further confirmed with UV-visible spectrophotometry. During the course of the reaction, the generation of $^{\cdot}OH$ was confirmed by the use of the chemical scavenger method. Briefly, thiourea or tertiary butanol was used, and no change in the color of the chromogenic substrate was observed.

This indirectly confirmed the role of the nanozyme in the generation of $^{\cdot}OH$, which subsequently works in the oxidation of TMB.

3.4. Optimization of different parameters

Several significant components affecting the sensor's efficiency were fine-tuned to improve its detection abilities and establish optimal operating conditions.

The amount of the Ag@bpp mimic enzyme was tested in the range of 1–2.2 mg, as shown in Fig. 5(i). The increase in the amount of the mimic enzyme resulted in the increase in activity till 1.8 mg, at which it showed the best performance. Hence, this amount of the mimic enzyme was used in the onward experiments. pH significantly influences the activity of biosensors; hence, it was optimized in the range of 3 to 9, as shown in Fig. 5(ii). The best performance of the proposed sensor was achieved at pH 5 and hence used for onward experiments. The concentration of TMB was optimized in the range of 1 and 7 mM, and the best response was observed at 4 mM. Hence, this amount of TMB was used for subsequent reactions. Finally, the
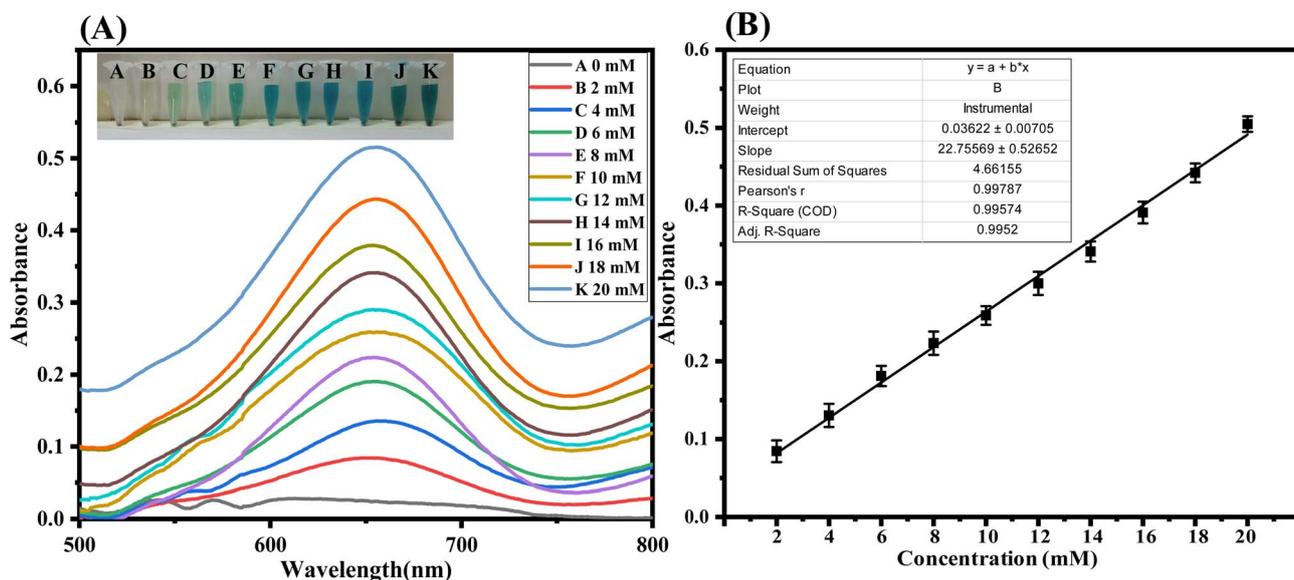

Fig. 6 (A) show UV-visible spectra of different cholesterol concentrations. (B) illustrate the calibration curve for the prepared nanosensor in the range of 0.1 to 1.8 mM.

Table 2 Comparative study of the fabricated sensor (Ag@bpp) with previously reported literature for the colorimetric sensing of cholesterol

| S. no.	Materials used	Method applied	Linear range (mM)	LOD (mM)	References
1	TiO_2	Colorimetric	0.1–50	61	49
2	Fe_2O_3/MNP	Colorimetric	0.39–6.47	0.194	50
3	TPU nanofibre/cellulose	Colorimetric	2–10	2	51
4	ChOx/Au@Ag NPs	Colorimetric	0.3–300	0.15	52
5	Cs:PVA NFs/GOxHRP/	Colorimetric	1.29–7.75	1.29	53
6	ChOx-MUDA-Fn-GNPs	Colorimetric	0.64–7.75	0.49	54
7	Fe_3O_4–GO	Colorimetric	0.047–0.952	0.041	32
8	CuO/G nanosphere composite	Colorimetric	0.1–0.8	0.78	55
9	Ag@bpp	Colorimetric	2–20	0.029	Present work
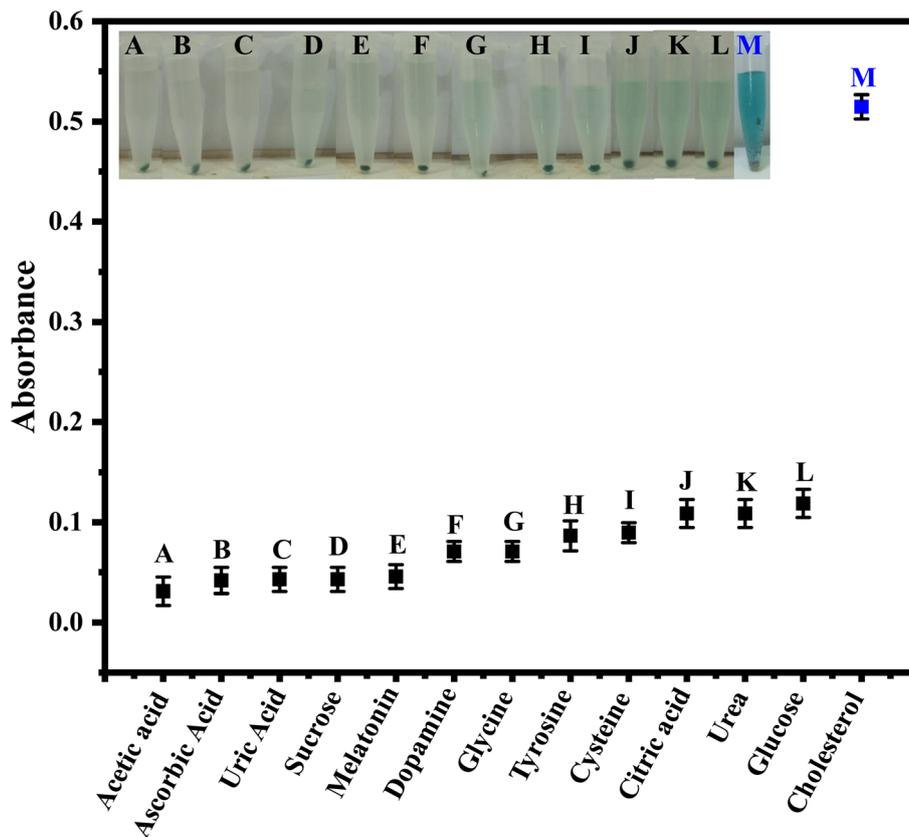
Fig. 7 Results of the interference experiments demonstrating the selectivity of the fabricated sensor towards cholesterol in the presence of equimolar concentrations of other species under the prevailing optimized conditions.

sensor system was optimized for response time in the range of 1 to 6 minutes. The optimal performance of the sensor was achieved at 4 minutes' time. Henceforth, the optimized time interval of 4 minutes was used.

3.5. Kinetic parameters assessment of the nanozyme

The synthesized mimic enzyme was studied for its kinetic properties in terms of key parameters, namely maximum velocity (V_{max}) and Michaelis constant, abbreviated as K_m. Its performance was compared with a natural enzyme, horseradish peroxidase (HRP). The results unveiled that the synthesized nanozyme has a comparable performance with that of the natural enzyme. The details can be seen in Table 1.

3.6. Analytical study of the fabricated sensor

The performance of the fabricated sensor was evaluated for the detection of cholesterol under the previously described optimum experimental conditions. As shown in Fig. 6, the amount of the analyte was progressively increased in a fixed ratio, and the change in absorbance was recorded. As shown in Fig. 6A, the increase in the concentration of cholesterol was performed in the range of 2–20 mM. However, above or below that mentioned level, the prepared sensor can detect the cholesterol; in contrast, the linearity response may not be achieved. Therefore, a calibration curve was drawn using the

aforementioned range of 2–20 mM, as seen in Fig. 6B. Moreover, according to calculations, the prepared sensor's limit of detection (LOD) and limit of quantification (LOQ) were 0.029 mM and 0.0957 mM, respectively. LOD and LOQ were calculated by using standard formulae $3 \times$ SD/slope and $10 \times$ SD/slope. The R square value was also calculated to be 0.995. In addition, Table 2 shows the comparison study of this prepared sensor with other reported literature for the colorimetric sensing of cholesterol.

Table 3 Application of the method to real samples using the standard addition method

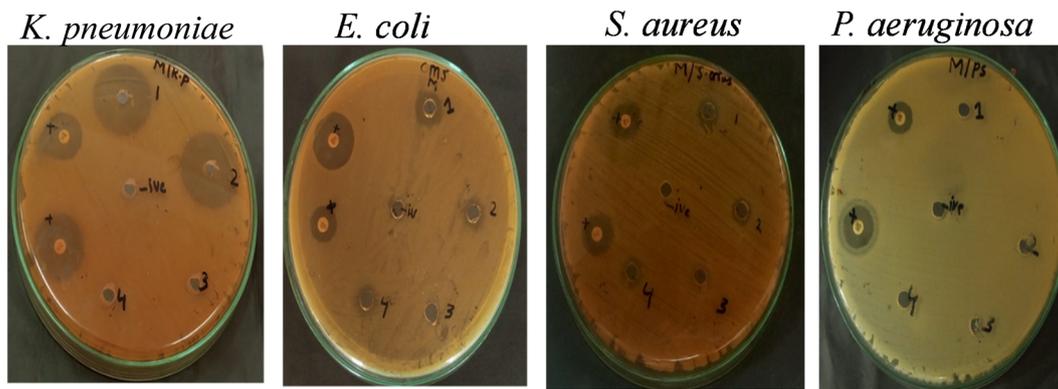| Cholesterol sample	Added, μM	Found, μM
Normal	0	5.02 ± 0.3
	5	10.12 ± 0.4
	6	11.00 ± 0.5
	7	12.05 ± 0.4
Moderately high	0	6.1 ± 0.1
	5	11 ± 0.3
	6	12.03 ± 0.4
	7	12.84 ± 0.5
High	0	7 ± 0.1
	5	11.86 ± 0.4
	6	13.01 ± 0.6
	7	13.7 ± 0.3

Fig. 8 Antibacterial activity of Ag@bpp (wells no. 1 and 2) against the selected bacterial strains showing its efficacy. Wells no. 3 and 4 represent the results of pristine BPP. DMSO was used as a negative control, while imipenem (10 µg) and gentamicin (10 µg) were run as positive controls.

3.7. Interference study

The proposed sensor's selectivity was explored by examining how it responded to a range of possible interfering species. These include acetic acid, ascorbic acid, uric acid, sucrose, melatonin, dopamine, glycine, tyrosine, cysteine, citric acid, urea, and glucose, as can be seen in Fig. 7. The findings of the study demonstrated that the fabricated sensor is highly selective for the detection of cholesterol under the prevailing optimized experimental conditions. The experiments were conducted using equimolar concentrations of cholesterol and the tested potential interfering species.

3.8. Application of the proposed sensor

To check the application of the proposed sensor, it was applied for the detection of cholesterol sensing in real samples using the standard addition method. For this purpose, real samples were collected and processed from normal, moderately high, and high cholesterol level individuals. The standard approach of method validation was used to calculate the precision and accuracy of the developed method. The real samples were processed and applied to the fabricated sensor under the reported optimal conditions. Table 3 shows the results of the real samples, and the values indicate the successful operation of the fabricated sensor for the detection of cholesterol in real samples.

3.9. Antimicrobial activities of the prepared nanocomposite

After establishing the role of the synthesized material Ag@bpp as a colorimetric sensing probe, its efficacy was tested as an antimicrobial agent. Various species of bacteria, such as *K. pneumoniae*, *E. coli*, *S. aureus*, and *P. aeruginosa*, were tested as shown in Fig. 8. Despite the use of a small amount of silver in the synthesized nanocomposite, it showed an excellent antibacterial potential against all the selected bacterial species. It shows that the selected combination of silver nanoparticles and the passive materials (bpp) in the selected ratio is a useful antibacterial agent. On one side it uses a small amount of silver nanoparticles, and on the other hand it utilizes biocompatible, low/no cost, ubiquitous, and biodegradable banana peel.

Imipenem (10 µg) and gentamicin (10 µg) were run as positive controls (+) to monitor the progress of the reactions. Pristine banana peel powder shown by well no. 3 and 4 was run to see its effect in solo. DMSO was used as a negative control as represented by negative (−ive) in the center of each plate. Ag@bpp was applied in well no. 1 and 2, and the results can be seen in the figure. Although these tests are not quantitative in the strict sense, they still show the antibacterial potential of the synthesized material. The best results could be observed for *K. pneumoniae* using the synthesized Ag@bpp nanocomposite.

4. Conclusions

In conclusion, the study reports on the successful synthesis of banana peel powder (bpp) and Ag@bpp nanocomposite. The comprehensive characterization through spectroscopic and morphological analyses techniques confirmed the desired synthesis of both bpp and Ag@bpp. The synthesized Ag@bpp nanocomposite was used as an oxidase and peroxidase mimic enzyme simultaneously for the colorimetric sensing of cholesterol without the use of hydrogen peroxide from any external source. The factors affecting the detection and quantification of cholesterol were optimized and were found to be 1.8 mg of the nanocomposite, PBS 400 µL (pH 5), TMB 80 µL (4 mM), time 4 minutes, and cholesterol 100 µL (20 mM). The fabricated sensor showed a wide linear range of 2–20 mM and LOD and LOQ values of 0.029 mM and 0.0957 mM, respectively, for cholesterol sensing. The selectivity study results showed no visible/considerable interference from various potential interfering species. The fabricated sensor was successfully used for the detection and quantification of cholesterol in real samples. The synthesized nanocomposite was also tested against various bacterial species such as *K. pneumoniae*, *E. coli*, *S. aureus*, and *P. aeruginosa*, with the best results achieved against *K. pneumoniae*. The fabricated sensor has the potential to be applied for diagnostic assessment and monitoring of cholesterol levels in the human body, food, and related applications.

Conflicts of interest

The authors declare no conflict of interest.

Data availability

The manuscript contains the majority of the data generated in the current work. Any additional information that may be required can be requested from the corresponding author on a reasonable basis.

Acknowledgements

References

1 N. M. Cerqueira, E. F. Oliveira, D. S. Gesto, D. Santos-Martins, C. Moreira, H. N. Moorthy, *et al.*, Cholesterol biosynthesis: a mechanistic overview, *Biochemistry*, 2016, **55**, 5483–5506.

2 N. R. Nirala, S. Abraham, V. Kumar, A. Bansal, A. Srivastava and P. S. Saxena, Colorimetric detection of cholesterol based on highly efficient peroxidase mimetic activity of graphene quantum dots, *Sens. Actuators, B*, 2015, **218**, 42–50.

3 G. Silbernagel, B. Schöttker, S. Appelbaum, H. Scharnagl, M. E. Kleber, T. B. Grammer, *et al.*, High-density lipoprotein cholesterol, coronary artery disease, and cardiovascular mortality, *Eur. Heart J.*, 2013, **34**, 3563–3571.

4 M. Balling, S. Afzal, A. Varbo, A. Langsted, G. Davey Smith and B. G. Nordestgaard, VLDL cholesterol accounts for one-half of the risk of myocardial infarction associated with apoB-containing lipoproteins, *J. Am. Coll. Cardiol.*, 2020, **76**, 2725–2735.

5 H. Lyu, D. Yin, B. Zhu, G. Lu, Q.-Y. Liu, X. Zhang, *et al.*, Metal-free 2 (3), 9 (10), 16 (17), 23 (24)-octamethoxyphthalocyanine-modified uniform CoSn (OH) 6 nanocubes: enhanced peroxidase-like activity, catalytic mechanism, and fast colorimetric sensing for cholesterol, *ACS Sustain. Chem. Eng.*, 2020, **8**, 9404–9414.

6 N. Nago, S. Ishikawa, T. Goto and K. Kayaba, Low cholesterol is associated with mortality from stroke, heart disease, and cancer: the Jichi Medical School Cohort Study, *J. Epidemiol.*, 2011, **21**, 67–74.

7 N. Zhang, Y. Liu, L. Tong, K. Xu, L. Zhuo and B. Tang, A novel assembly of Au NPs–β-CDs–FL for the fluorescent probing of cholesterol and its application in blood serum, *Analyst*, 2008, **133**, 1176–1181.

8 M. Amiri and S. Arshi, An overview on electrochemical determination of cholesterol, *Electroanalysis*, 2020, **32**, 1391–1407.

9 H. Arshad, M. Chaudhry, S. Mehmood, A. Farooq, M. Wang and A. Bhatti, The electrochemical reaction controlled optical response of cholestrol oxidase (COx) conjugated CdSe/ZnS quantum dots, *Sci. Rep.*, 2020, **10**, 20439.

10 M. P. Pešić, M. D. Todorov, G. Becskereki, G. Horvai, T. Ž. Verbić and B. Tóth, A novel method of molecular imprinting applied to the template cholesterol, *Talanta*, 2020, **217**, 121075.

11 T. G. Albuquerque, M. B. P. Oliveira, A. Sanches-Silva and H. S. Costa, Cholesterol determination in foods: Comparison between high performance and ultra-high performance liquid chromatography, *Food Chem.*, 2016, **193**, 18–25.

12 X.-S. Miao and C. D. Metcalfe, Determination of cholesterol-lowering statin drugs in aqueous samples using liquid chromatography–electrospray ionization tandem mass spectrometry, *J. Chromatogr. A*, 2003, **998**, 133–141.

13 R. Ahmad, N. Tripathy and Y.-B. Hahn, High-performance cholesterol sensor based on the solution-gated field effect transistor fabricated with ZnO nanorods, *Biosens. Bioelectron.*, 2013, **45**, 281–286.

14 M. J. Chaichi and M. Ehsani, Determination of glucose and cholesterol using a novel optimized luminol-CuO nanoparticles-H_2O_2 chemiluminescence method by Box–Behnken design, *J. Fluoresc.*, 2015, **25**, 861–870.

15 Q. Zhang, G. Fan, W. Chen, Q. Liu, X. Zhang, X. Zhang, *et al.*, Electrochemical sandwich-type thrombin aptasensor based on dual signal amplification strategy of silver nanowires and hollow Au–CeO_2, *Biosens. Bioelectron.*, 2020, **150**, 111846.

16 Y. Yang, X. Niu, B. Duan, J. Lu and X. Zhang, Dual-modal biosensor for mercuric ion detection based on $Cu_2O@Cu_2S$/D-TA COF heterojunction with excellent catalase-like, electrochemical and photoelectrochemical properties, *Biosens. Bioelectron.*, 2024, **262**, 116568.

17 M. Asad, N. Muhammad, N. Khan, M. Shah, M. Khan, M. Khan, *et al.*, Colorimetric acetone sensor based on ionic liquid functionalized drug-mediated silver nanostructures, *J. Pharm. Biomed. Anal.*, 2022, **221**, 115043.

18 U. Nishan, A. Ahmed, N. Muhammad, M. Shah, M. Asad, N. Khan, *et al.*, Uric acid quantification via colorimetric detection utilizing silver oxide-modified activated carbon nanoparticles functionalized with ionic liquid, *RSC Adv.*, 2024, **14**, 7022–7030.

19 J. Lian, P. Liu and Q. Liu, Nano-scale minerals in-situ supporting CeO_2 nanoparticles for off-on colorimetric detection of L–penicillamine and Cu^{2+} ion, *J. Hazard. Mater.*, 2022, **433**, 128766.

20 R. Ullah, M. Soylak, M. Asad, M. Khan, M. Shah, N. Khan, *et al.*, Manganese oxide-doped graphitic carbon nitride-based 2D material as nanozyme for the colorimetric sensing of ascorbic acid, *Sens. Actuators, A*, 2024, **380**, 115995.

21 U. Nishan, I. Ullah, N. Muhammad, S. Afridi, M. Asad, S. U. Haq, *et al.*, Investigation of silver-doped iron oxide nanostructures functionalized with ionic liquid for colorimetric sensing of hydrogen peroxide, *Arabian J. Sci. Eng.*, 2023, **48**, 7703–7712.

22 D. Bae, M. Kim and J.-s. Choi, Enzymatic properties of iron oxide nanoclusters and their application as a colorimetric glucose detection probe, *RSC Adv.*, 2025, **15**, 4573–4580.

23 Y. Zhang, P. Liu, S. Xie, M. Chen, M. Zhang, Z. Cai, et al., A novel electrochemical ascorbic acid sensor based on branch-trunk Ag hierarchical nanostructures, J. Electroanal. Chem., 2018, 818, 250–256.

24 J. Lu, H. Zhang, S. Li, S. Guo, L. Shen, T. Zhou, et al., Oxygen-vacancy-enhanced peroxidase-like activity of reduced Co_3O_4 nanocomposites for the colorimetric detection of H_2O_2 and glucose, Inorg. Chem., 2020, 59, 3152–3159.

25 L. Wang, Z. Liu, Q. Yang, M. Xie and Q. Liu, Sustainable phthalocyanine-modified TiO2 nanofilm as a light-operated nanozyme for colorimetric determination of L-penicillamine, ACS Sustainable Chem. Eng., 2024, 12, 2203–2211.

26 J. Lian, P. Liu, C. Jin, Q.-Y. Liu, X. Zhang and X. Zhang, Flower-like CeO_2/CoO p–n heterojuncted nanocomposites with enhanced peroxidase-mimicking activity for l-cysteine sensing, ACS Sustain. Chem. Eng., 2020, 8, 17540–17550.

27 M. Asad, N. Khan, M. Khan, M. Shah, W. Sun, X. Zhang, et al., Ionic liquid-capped silver-zinc oxide@activated carbon: A Powerful nanocomposite for colorimetric uric acid detection, J. Photochem. Photobiol., A, 2025, 463, 116273.

28 E. Fabre, C. B. Lopes, C. Vale, E. Pereira and C. M. Silva, Valuation of banana peels as an effective biosorbent for mercury removal under low environmental concentrations, Sci. Total Environ., 2020, 709, 135883.

29 A. Stavrinou, C. Aggelopoulos and C. Tsakiroglou, Exploring the adsorption mechanisms of cationic and anionic dyes onto agricultural waste peels of banana, cucumber and potato: Adsorption kinetics and equilibrium isotherms as a tool, J. Environ. Chem. Eng., 2018, 6, 6958–6970.

30 C. R. Silva, T. F. Gomes, G. C. Andrade, S. H. Monteiro, A. C. Dias, E. A. Zagatto, et al., Banana peel as an adsorbent for removing atrazine and ametryne from waters, J. Agric. Food Chem., 2013, 61, 2358–2363.

31 M. Alle, R. Bandi, G. Sharma, R. Dadigala, S.-H. Lee and J.-C. Kim, Gold nanoparticles spontaneously grown on cellulose nanofibrils as a reusable nanozyme for colorimetric detection of cholesterol in human serum, Int. J. Biol. Macromol., 2022, 201, 686–697.

32 J. Singh, R. Singh, S. Singh, K. Mitra, S. Mondal, S. Vishwakarma, et al., Colorimetric detection of hydrogen peroxide and cholesterol using Fe_3O_4-brominated graphene nanocomposite, Anal. Bioanal. Chem., 2022, 414, 2131–2145.

33 S. Li, L. Liang, L. Tian, J. Wu, Y. Zhu, Y. Qin, et al., Enhanced peroxidase-like activity of MOF nanozymes by co-catalysis for colorimetric detection of cholesterol, J. Mater. Chem. B, 2023, 11, 7913–7919.

34 J. Li, T. Liu, R. A. Dahlgren, H. Ye, Q. Wang, Y. Ding, et al., N, S-co-doped carbon/$Co_{1-x}S$ nanocomposite with dual-enzyme activities for a smartphone-based colorimetric assay of total cholesterol in human serum, Anal. Chim. Acta, 2022, 1204, 339703.

35 M. V. Kuznetsova, L. Y. Nesterova, V. S. Mihailovskaya, P. A. Selivanova, D. A. Kochergina, M. O. Karipova, et al., Nosocomial Escherichia coli, Klebsiella pneumoniae, pseudomonas aeruginosa, and staphylococcus aureus:

Sensitivity to chlorhexidine-based biocides and prevalence of efflux pump genes, Int. J. Mol. Sci., 2025, 26, 355.

36 J. Denissen, B. Havenga, B. Reyneke, S. Khan and W. Khan, Comparing antibiotic resistance and virulence profiles of Enterococcus faecium, Klebsiella pneumoniae, and Pseudomonas aeruginosa from environmental and clinical settings, Heliyon, 2024, 10, e30215.

37 M. Riaz, V. Mutreja, S. Sareen, B. Ahmad, M. Faheem, N. Zahid, et al., Exceptional antibacterial and cytotoxic potency of monodisperse greener AgNPs prepared under optimized pH and temperature, Sci. Rep., 2021, 11, 2866.

38 S. Ullah, W. Sun, X. Zhang, M. Asad, M. Ahmad, R. Ullah, et al., Colorimetric detection of dopamine using banana peel powder-deposited manganese dioxide nanoparticles, Waste Biomass Valorization, 2025, 1–12.

39 S. Kamsonlian, S. Suresh, C. Majumder and S. Chand, Characterization of banana and orange peels: biosorption mechanism, Int. J. Serv. Sci. Manag. Eng. Technol., 2011, 2, 1–7.

40 H. Manivannan and B. L. Anguraj, Valorization of fruit waste using DES pretreatment and hydrolysis over a heterogeneous catalyst for bioethanol production, Biomass Convers. Biorefin., 2023, 13, 5731–5741.

41 D. Garibo, H. A. Borbón-Nuñez, J. N. D. de León, E. García Mendoza, I. Estrada, Y. Toledano-Magaña, et al., Green synthesis of silver nanoparticles using Lysiloma acapulcensis exhibit high-antimicrobial activity, Sci. Rep., 2020, 10, 12805.

42 R. Singh and B. Datta, Banana peel powder as an effective multilayer adsorbent of ammonium ions, Ind. Eng. Chem. Res., 2022, 61, 18464–18474.

43 T. Zeng, M. Yu, H. Zhang, Z. He, J. Chen and S. Song, Fe/Fe_3C@ N-doped porous carbon hybrids derived from nano-scale MOFs: robust and enhanced heterogeneous catalyst for peroxymonosulfate activation, Catal. Sci. Technol., 2017, 7, 396–404.

44 T. Guo, K. Wang, G. Zhang and X. Wu, A novel α-Fe_2O_3@g-C_3N_4 catalyst: synthesis derived from Fe-based MOF and its superior photo-Fenton performance, Appl. Surf. Sci., 2019, 469, 331–339.

45 W. Chen, C. Hu, Y. Yang, J. Cui and Y. Liu, Rapid synthesis of carbon dots by hydrothermal treatment of lignin, Materials, 2016, 9, 184.

46 W. Lu, X. Qin, A. M. Asiri, A. O. Al-Youbi and X. Sun, Green synthesis of carbon nanodots as an effective fluorescent probe for sensitive and selective detection of mercury (II) ions, J. Nanopart. Res., 2013, 15, 1–7.

47 J. C. Martínez Espinosa, R. Carrera Cerritos, M. A. Ramírez Morales, K. P. Sánchez Guerrero, R. A. Silva Contreras and J. H. Macías, Characterization of silver nanoparticles obtained by a green route and their evaluation in the bacterium of Pseudomonas aeruginosa, Crystals, 2020, 10, 395.

48 X. Wang, C.-L. Tang, J.-J. Liu, H.-Z. Zhang and J. Wang, Ultra-small CuS Nanoparticles as Peroxidase Mimetics for Sensitive and Colorimetric Detection of Uric Acid in Human Serum, Chin. J. Anal. Chem., 2018, 46, e1825–e1831.

49 R. Rathinam, D. P. Singh, A. Dutta, S. Rudresha, S. R. Ali and P. Chatterjee, TiO$_2$ Nanoparticles Based Peroxidase Mimics for Colorimetric Sensing of Cholesterol and Hydrogen Peroxide, *Adv. Sci. Technol.*, 2022, **117**, 85–90.

50 D. Cho and H. G. Park, Colorimetric quantification of glucose and cholesterol in human blood using a nanocomposite entrapping magnetic nanoparticles and oxidases, *J. Nanosci. Nanotechnol.*, 2015, **15**, 7955–7961.

51 S. Immanuel, V. Elakkiya, M. Alagappan and R. Selvakumar, Development of colorimetric cholesterol detection kit using TPU nanofibre/cellulose acetate membrane, *IET Nanobiotechnol.*, 2018, **12**, 557–561.

52 X. Zhang, M. Wei, B. Lv, Y. Liu, X. Liu and W. Wei, Sensitive colorimetric detection of glucose and cholesterol by using Au@Ag core–shell nanoparticles, *RSC Adv.*, 2016, **6**, 35001–35007.

53 M. Dhawane, A. Deshpande, R. Jain and P. Dandekar, Colorimetric point-of-care detection of cholesterol using chitosan nanofibers, *Sens. Actuators, B*, 2019, **281**, 72–79.

54 N. R. Nirala, P. S. Saxena and A. Srivastava, Colorimetric detection of cholesterol based on enzyme modified gold nanoparticles, *Spectrochim. Acta, Part A*, 2018, **190**, 506–512.

55 V. Sharma and S. M. Mobin, Cytocompatible peroxidase mimic CuO: graphene nanosphere composite as colorimetric dual sensor for hydrogen peroxide and cholesterol with its logic gate implementation, *Sens. Actuators, B*, 2017, **240**, 338–348.